Pure Appl. Geophys. 168 (2011), 1835–1849

DOI 10.1007/s00024-010-0189-7

Pure and Applied Geophysics

Structural Setting of Northern Tunisia Insights from Gravity Data Analysis Jendouba Case Study

Imen Hamdi Nasr,[1] Adnen Amiri,[1] Mohamed Hédi Inoubli,[1] Abdelhmid Ben Salem,[1] AbdelHak Chaqui,[1] and Said Tlig[1]

Abstract—Detailed gravity data in conjunction with available surface geology are analyzed to infer the organization of the underlying structures in Jendouba area. Gravity data analysis benefits from the gravity Bouguer anomaly, upward continuations, residual distribution, derivatives and Euler deconvolved maps. The main results display a positive amplitude gravity anomaly as the response of Triassic evaporitic bodies and important NE trending features at the boundaries between the Triassic outcrops and their enveloping strata. Integration of gravity, geological and structural maps let to the identification of major structural directions and trends of the study area. It confirms some structural elements gathered from outcrops. It defines also new ones.

Key words: Gravity, fault, triassic, dome, positive anomaly, Tunisia, Bouguer, gradient, mapping.

1. Introduction

Northern Tunisian Atlas pertains to the Alpine fold belts surrounding the western Mediterranean and the Alboran Sea; it extends to the straits of Sicily to the East. To the West, it can be recognized across northern Algeria and the Moroccan Rif. The structural style and the role of thrusting in the structural evolution of this fold belt in Tunisia remain a controversy.

Much of the published literature emphasized the important role of diapirism associated to Triassic strata in northern Tunisia; diapirism has been influencing the structural architecture (Perthuisot, 1978), at least as from the Aptian.

Diapiric zone is characterized by NE elongated chaotic strata leading to their tectonic contact with a bunch of series laying from Lower Cretaceous to Miocene rocks.

Northern Tunisia constitutes the north-eastern edge of the African plate. It is bordered by the Mediterranean Sea and the Straight of Sicily to the north and north-east, with an uppermost crust bearing Meso-Cenozoic prevalent sedimentary packages that have all along suffered Alpine and Atlassic orogenies (Castany, 1952; Crampon, 1973; Rouvier, 1977; Cohen *et al*., 1980; Tlig *et al*., 1991). In the region, an Early Mesozoic rifting phase has structured basin sunk salt dominated Triassic deposits, and was seconded by a passive margin tectonic basin style during the entire meso-cenozoic times. Moreover, Northern Tunisia has been the subject of several gravity data analysis (Jallouli *et al*., 2002; Jallouli *et al*., 2005; Inoubli and Mansouri, 2006; Benassi *et al*., 2006; Robinson *et al*., 2007; Hamdi Nasr *et al*., 2008; Hamdi Nasr *et al*., 2009).

The main objective of this paper is to correlate gravity anomalies and their derivatives with the known surface geology while investigating the subsurface geological structure.

These goals are achieved through data analysis using potential field transformations and interpretation techniques and the application of the Euler deconvolution method to gravity data.

2. Geological Setting

The study area is located in the northern Tunisian Atlas (Fig. 1), which is characterized by numerous NE-trending outcrops of Triassic rocks. Jendouba map contains three major salty outcrops (Fig. 2): Ragoubet Elhanech Triassic band, Fedj el adoum

[1] Faculté des Sciences de Tunis, UR-GAMM, Université Tunis-El Manar, El Manar, 2092 Tunis, Tunisia. E-mail: imenhamdi79@yahoo.fr

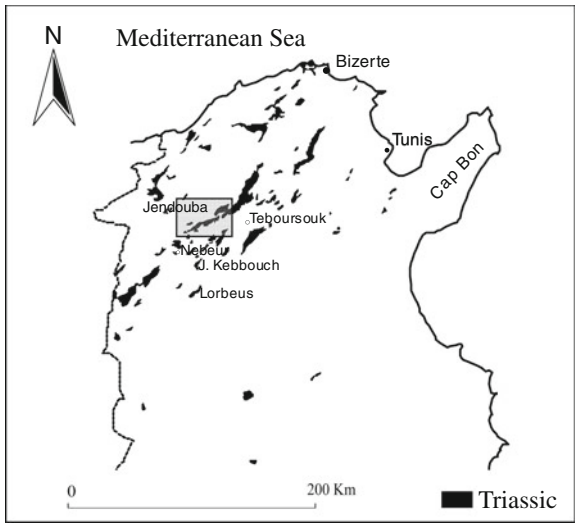

Figure 1
Location of the study area

Triassic band and the NE trending 25 km large and elongated Djebba-Souk es Sebt Triassic band. The latter is bounded on its northern flank by Neogene series; its southern flank is limited by Cretaceous sediments. On the western part of the map, Triassic drowns down under Neogene and Quaternary sediments. Cretaceous sediments are cut by NW trending faults and lie unconformably over the Triassic rocks.

The Triassic rocks consist of evaporates with thin layers of clay, sands, limestone, dolostones together with some metasomatized basalts (sills, dikes). Cretaceous sequences varies from compact limestone to marls, whereas the Cainozoic sequence consists of clays, marls and sands. These sequences are affected by numerous faults trending NW and NS.

During Late Cretaceous and Cainozoic, northern Tunisia was affected by a series of compressional events caused by the northward movement of the African plate with the most prominent event occurring during the Late Miocene. Such tectonic events played a role in the rising of the Triassic evaporitic rocks and controlled the overall structure of the region.

3. Gravity Data

In this study, high-resolution gravity data in the northern Tunisian Atlas collected by the "Office National des Mines" (ONM) were used. Acquisition was carried out in 1997 by the ValDor Sagax Company. Gravity data cover the 1/50,000 scale map of Jendouba. Six hundred and sixty measurements were performed on a 640 km^2 area. The studied area is covered by gravity stations on an almost 1 × 1 km^2 grid. Positioning and station elevation were determined using

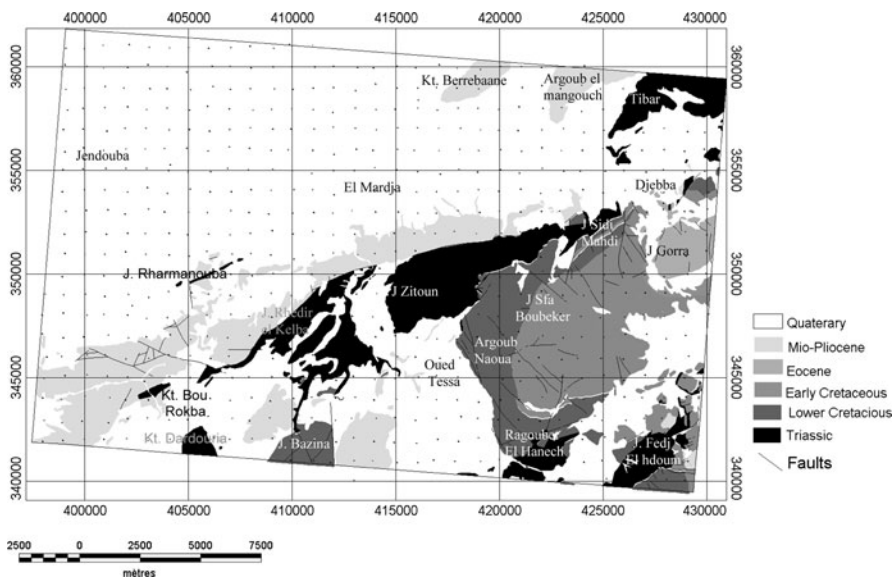

Figure 2
Geologic map of the study area

global positioning system GPS (Leica) in a differential mode. Adopted projection is Lambert North using the Clark ellipsoid 1880 and Carthage datum. Free-air and Bouguer gravity corrections were performed using sea level as a datum and a reduction density of 2.4 g cm^3. The choice of this value results from the comparison of the results from several methods (ONM, 2000).

- Direct measurement of densities done on 150 samples coming from five mining wells provided by ONM. The average bulk density has been valued to 2.4 g/cm^3.
- The indirect method was performed using Nettleton profiles: three profiles were acquired. They have been realized over representative formations of the area of study and presenting an important altitude difference. The Bouguer anomaly profiles were computed using eight density values ranging from 2.36 to 2.5 using a sampling rate of 0.02. A 2.4 density value leads to the least topographic contaminated profiles. Moreover, the good correlation between the density derived from Nettleton and those measured allowed choosing a regional density of 2.4 g/cm^3.

Bouguer and terrain corrections were calculated automatically using a digital elevation model obtained by digitizing 1/50,000 scale topographic maps. Taking into account the quality of the gravity and positioning measurements, we found that the accuracy of the survey is around 0.02 m Gal for gravity measurements and 0.1 m for the positioning of the stations. The near zones topographic corrections—zone A to zone C—(HAMMER 1939) were calculated after direct evaluation of local topographic variation. The faraway corrections—D zone to M zone—were determined using the previously determined DEM. A quality control of the topographic data digitization was performed through comparison with the acquired GPS data.

4. Bouguer Anomaly

Bouguer gravity anomaly maps are commonly used to investigate subsurface geology and structures (BLAKELY and SIMPSON, 1986). The observed complete Bouguer gravity anomalies reflect the effect of all density heterogeneities beneath the surface.

The complete Bouguer gravity anomaly values range from −15 to +13 m Gal (Fig. 3). The outcrop pattern of the Triassic rocks has been digitized from the 1/50,000 scale geological map of BEN HAJ ALI *et al*., (1997) and superimposed onto the complete Bouguer gravity map.

Positive anomalies are placed in the central eastern part of the map. The most important one is slightly spliced to the south; it coincides with Triassic and Cretaceous outcrops at Jebel El Zitoun, Sidi el Mahdi, Jebel Argoub Naoua and Jbel Sfa Boubakrer zones. The maximum amplitude occurs over the lower cretaceous outcrops. The anomaly sited over El Merdja zone express less amplitude and extension than the previous one.

The positive anomaly of Argoub Naoua-Sfa BouBeker is distinguishable by its high amplitude. This is related to the limy and marly series of the lower cretaceous which are characterized by significantly high density values.

Negative anomalies are located mainly in the west to northwestern part of the map; it is sensitive to indicate that all this area is covered by the non compacted deposits of the Medjerda River discharges which are Quaternary in age. The overall Medjerda plain expresses negative gravity values with almost two different wavelengths (−13.4 m Gal and almost −1.1 m Gal).

Triassic response is variable: slightly positive at the level of Thibar, strong positive response in Djebel Zitoun and slightly negative in J. Rhdir el Kelba. This variety of gravity responses can be explained by the influence of the structures next these Triassic outcrops.

5. Data Processing and Transformation

Gravity anomaly maps exhibit the combined effects of geologic bodies of distinctive densities, their shape, their lateral extension, and their depth of burial. The gravity field is the superposition of signals in close connection with the above defined parameters. In order to accentuate the shallow source anomalies, a continuation filtering process which is designed lead to a separation of long wavelength anomalies from short wavelength ones was applied.

The decomposition of the gravity signal depends on the depth of sources; it allows the identification of

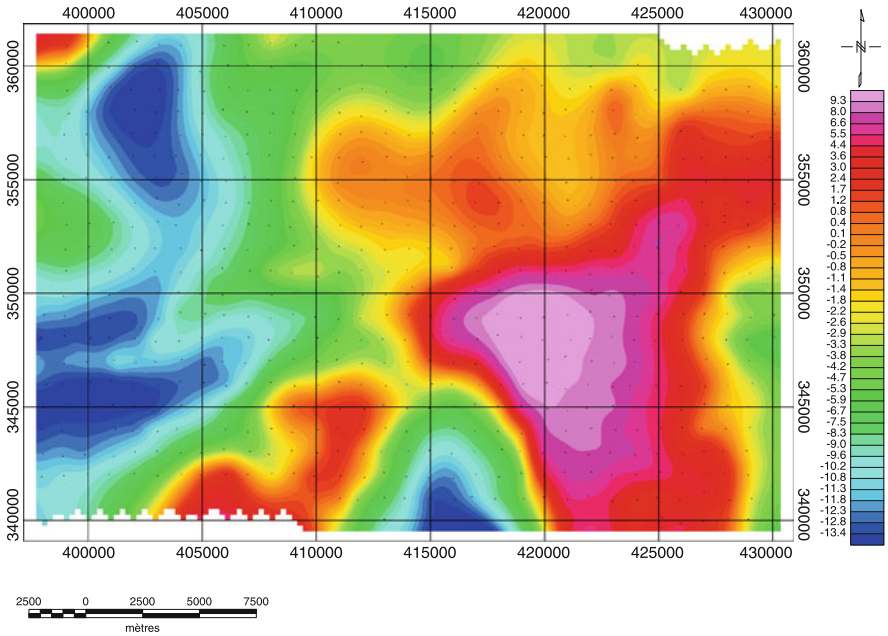

Figure 3
Bouguer anomaly map

the structures and to recognize their spatial arrangement. Thus, transformations of the field data which are often helpful for general qualitative as well as quantitative interpretation have been realized: In this study, the processes applied, and products used, include upward continuation and vertical and horizontal gradients (Fig. 3).

In any region of space which do not contain the source, upward continuation of the observed potential field is described in the spatial domain by the expression (Jacobsen, 1987):

$$U(x,y,z_0-\Delta z) = \frac{\Delta z}{2\pi}\int\int \frac{U(x',y',z_0)}{\left[(x-x')^2+(y-y')^2+\Delta z^2\right]^{3/2}}\mathrm{d}x'\mathrm{d}y',\ \Delta z \succ 0.$$

U is the potential field; z_0 is the observation plane; Δz is the upward continuation distance. z is positive downward.

In the Fourier domain, the transformation becomes a simple multiplication:

$$\mathrm{F}[U_p] = \mathrm{e}^{-\Delta z|k|}\mathrm{F}[U]$$

F represents the Fourier transformation, U_p is the continued field, k is the radial wavenumber (radian/km).

The exponential factor constitutes the upward continuation operator. This operator attenuates the amplitude of the field components according to their wavenumbers. For the elevated wavenumbers, the operator stretches toward zero, and succeeds to important reduction of the amplitude of short wavelengths of the field components (Blakely, 1996). Inverse Fourier transformation constitutes the continued field. Therefore, the deeper the sources the more important will be their weight. Thus, upward continuation may be used for regional field construction.

In this case study, upward continuation was applied for different elevation values. Compared the complete Bouguer anomaly, to isogal curves are smoother. Quite some positive anomalies merge into a unique, simple and regular anomaly which migrates to the East. Negative anomalies fused also in the western part of the area. The isogal curves become parallel, defining an ENE-WSW oriented regional gradient, from a 28 km level upward continuation.

Separation of regional and residual anomalies is conventionally one of the most difficult tasks (Gupta and Ramani, 1980). It constitutes, in the mean time, an essential part of potential field interpretation; a number of techniques are available including graphical and/or visual methods, wavelength filtering,

spectral analysis, and upward continuation (BLAKELY, 1996).

The present case study regional component (BLAKELY and SIMPSON, 1986; JACOBSEN, 1987) was computed through upward continuing the Bouguer gravity grid to 28 km; it is relevant to indicate that for higher continuation levels, the extracted map shape is almost unchanged. As the average crustal thickness approximates 28 km (BUNESS *et al.*, 1992), the indicated upward continuation level suggests the isolation of an equivalent 14 km thick layer (JACOBSEN, 1987).

Therefore, a residual gravity map (Fig. 4) was computed by subtracting the regional grid from the Bouguer gravity grid. Derivative maps were also computed in order to enhance the short wavelength features that usually correspond to shallow elements of geology.

The residual gravity anomaly map express shorter wavelength anomalies with values ranging between −3 and +4 m Gal. High amplitude maxima are located in central, northeastern and southeastern parts of the map and occur over known outcrops of Triassic and the lower Cretaceous intervals. In contrast, low amplitude anomalies are located in the southwestern and the northwestern parts superimposed to Quaternary deposits.

A closer examination of the residual gravity anomalies lead to the subdivision of the studied area into six gravity anomaly regions based on the trend, the wavelength and the amplitude of the anomaly (Fig. 4).

Region 1 is mainly made of large scale gravity anomaly; it is basically the highest amplitude response. It is directed N–S, occurring mostly over Triassic outcrops and lower Cretaceous sedimentary units, with marls and sandstone (BEN HAJ ALI, 1979) (Fig. 2). This corresponds to Argoub Naoua and Djebel Sfa Bou Beker. Its western limit is truncated by the large amplitude gravity minima of region 6.

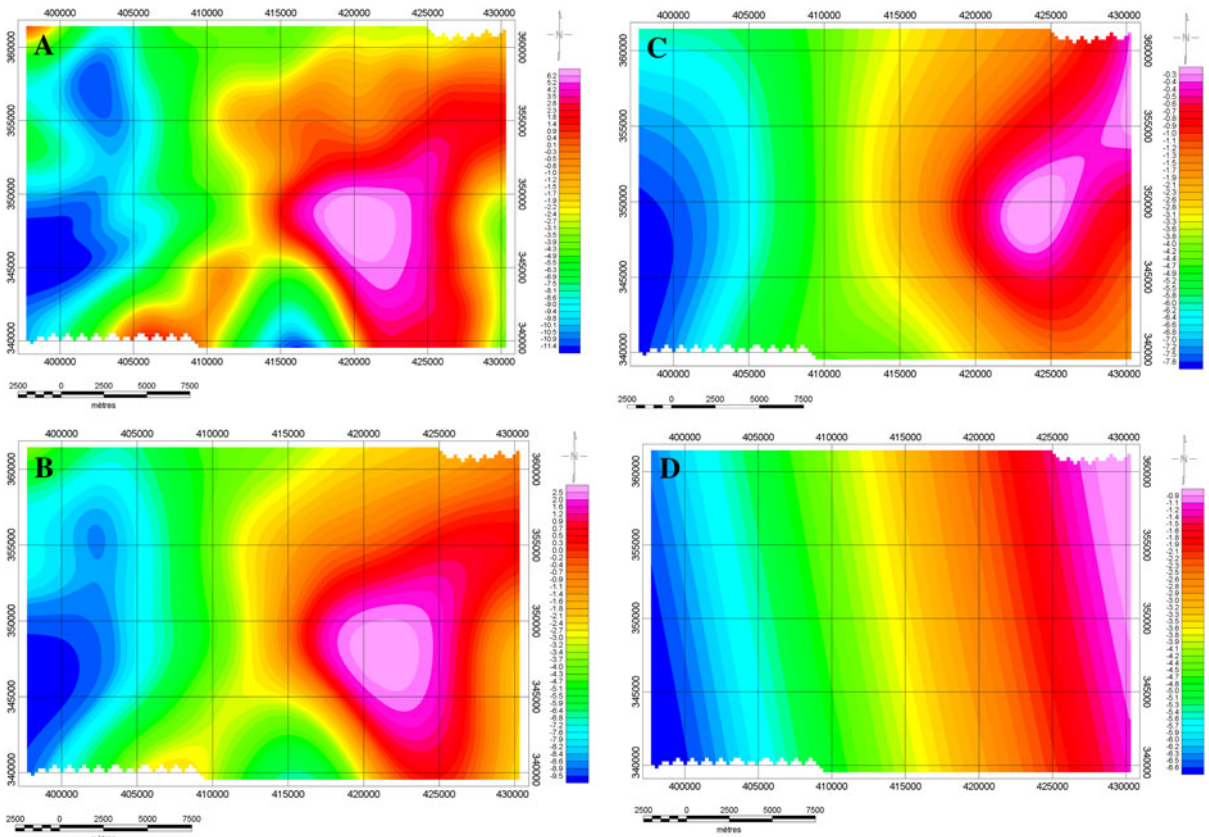

Figure 4
Upward continuation **a** 1,000 m, **b** 5,000 m, **c** 7,000 m, **d** 28,000 m

Region 2 is positive and mostly trending north to northeast with a small extension to the west that principally coincides with the early Cretaceous outcrops of Jebel Ghazouane (Fig. 1). This region extends also to the south west.

Region 3 corresponds to the circular anomaly of El Mardja. This large scale gravity response occurs mostly over Quaternary deposits and is located at the western edge of the Majerda River. This anomaly expands laterally by thin elongated EW to NE directed positive gravity response. As the surface Quaternary series cannot explain such anomaly, this suggests the presence of dense and deeper units.

Region 4 has NE and SE extensions, it represent a negative anomaly centered on the Majerda River. Thick recent Quaternary deposits cover this area.

Region 5 corresponds to a negative elongated EW oriented anomaly. It is superimposed to the Mio-Pliocene and Quaternary outcropping sediments.

Region 6 is a large scale gravity minimum directed N–S. It occurs mostly over Quaternary and Mio-Pliocene deposits.

6. Gravity Gradients

In order to delineate a lateral boundary due to the main sources of gravity responses, edge enhancement techniques based on gravity signal derivatives—horizontal and vertical gradients, analytical signals—were also used. These techniques are utilized to locate the lateral boundaries of density contrasts and provide information on the location of geological units (Blakely and Simpson, 1986; Phillips Jeffrey *et al*., 2007).

The horizontal derivative of the potential field has been used to image the boundaries of potential field sources (Blakely and Simpson, 1986). A number of other boundary estimators where defined following the concept of normalized derivatives, e.g. Verduzco *et al*., 2004; Cooper and Cowan, 2006; Fairhead and Williams, 2006; Phillips *et al*., 2007. A quite different approach, based on a generalized concept of horizontal derivative, named enhanced horizontal derivative (EHD), (Fedi and Florio, 2001). It is a high resolution boundary estimator based on the horizontal derivative of a weighted sum of field vertical derivatives:

$$\mathrm{EHD}(x,y) = \sqrt{\left[\left(\frac{\partial\phi}{\partial x}\right)^2 + \left(\frac{\partial\phi}{\partial y}\right)^2\right]}$$

where,

$$\phi(x,y) = f(x;y) + w_1 f^{(1)}(x,y) + w_2 f^{(2)}(x,y) + \ldots + w_m f^{(m)}(x,y)$$

Here $f^{(m)}$ being the m^{th} order vertical derivative of the field (m is ranging from 1 to 7) and w_m being a set of weights. The higher vertical derivatives lead to a better detail of the shallower sources. Weights control the relative importance of the terms of the summation. When conveniently chosen, they allow different-scale lineaments to be satisfactorily enhanced. This technique can be defined with a great flexibility in relation with the noise characteristics of the field to be analyzed and, more interestingly, in relation with the wanted detail. For example, the low order terms may include also the first vertical integral of the field, and the enhanced gradient will allow to image regional-scale structures (Fedi *et al*., 2007). This total gradient will peak over all isolated 2-D sources and over some 3-D sources; it can be used as a special function to estimate horizontal locations and strike of the sources (Phillips *et al*., 2007).

The previously defined geological details are recognizable in the EHD map (Fig. 5). The map seems to be subdivided into two areas through an important and strong well defined NE lineament covering the elongated Triassic band Tibar–J. Sidi Mahdi–J. Zitoun–J. Rhedir El kalba–Kt. Bou Rokba. The southern area mostly expresses regions with gravity maxima.

The Northern area is covered mainly by Quaternary sediments. The low relief positive gradients, expressed in some localities, reflect deeper lateral density contrasts. This is the case of El Mardja anomaly which is bordered to the North East by a NE directed gradient. Another one is marked by a positive gradient expressed at Kt. Berrebaane. To the Northwestern part of the map, there is emergence of NNE directed gradient characterized by alternating positive and negative lineaments.

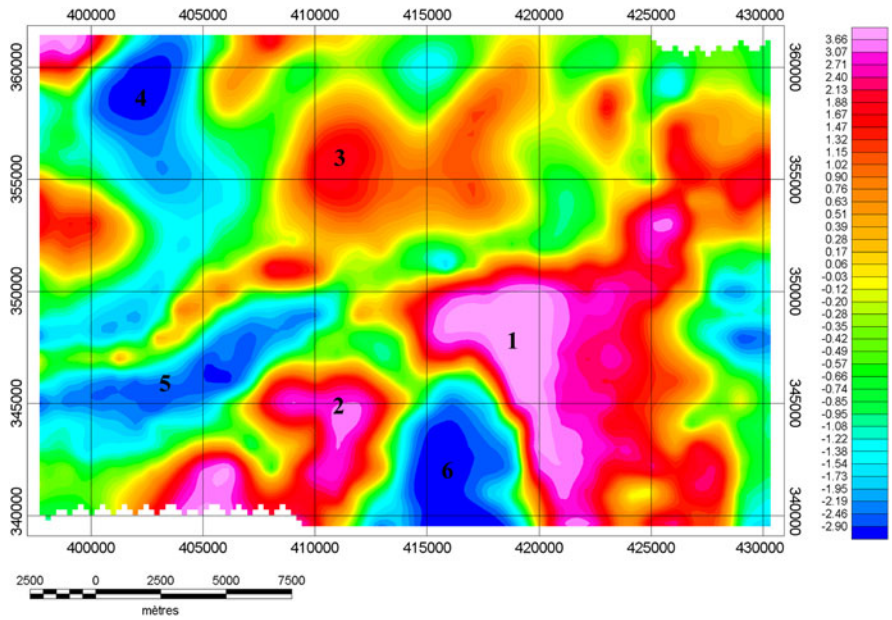

Figure 5
Residual gravity anomaly map

The EHD method succeeded on the definition of source boundaries. This technique conveys efficiently all the different boundary information contained in any single term of the sum.

The second vertical derivative map (Fig. 6) high lights the NS trending of the borders of the lower Cretaceous of Argoub nawa Sfa Boubeker. It indicates also the EW and SW lineaments expressed by the Triassic outcrops of J. Rharmanouba.

The maximum value of the horizontal gravity gradient (HGG) tends to be located on the horizontal edges of the gravity sources marked by rapid changes

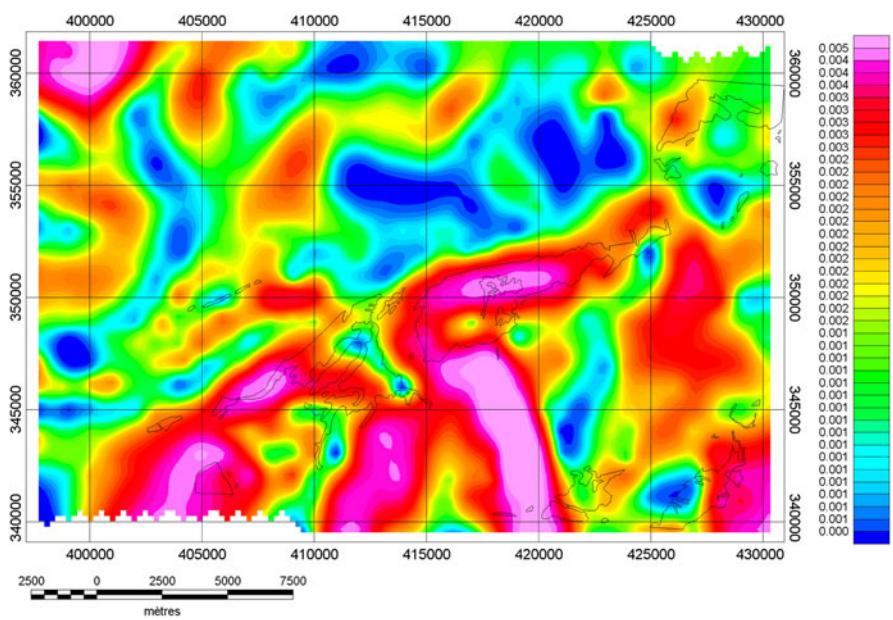

Figure 6
Enhanced horizontal gradient

in density values (BLAKELY, 1996). The Horizontal directionally dependent gradient consists on the application of a 3 × 3 point convolution filter to the gravity grid. The nine point filter depends on the specified gradient direction. The HGG map (Fig. 7) was computed using Geosoft/Oasis Montaj software specifying a gradient direction perpendicular to the regional structural direction (70°N) defined by surface geology. The map expresses a variety of thin, but stretched out alignments; the most significant of which is surrounding the Triassic outcrops. Thus, there is tentative evidence that these might reflect lateral density contrast between the extruded Triassic evaporitic bodies and the surrounding rocks. In the region of J. Rhedir el Kelba, gravity lineament over Triassic outcrops continues to the West. It is separated by a gravity low from another gravity high that partially coincides with Triassic outcrops of J. Rharmanouba. To the North, this direction is also well expressed through its gravity high over the Mio-Pliocene deposit of Kt. Berrebaane. It is sensitive to outline its presence within all transformed gravity maps (EHG, HGG, and second Vertical gradient maps). However, it has the best expression in the HGG map.

Horizontal and vertical gradients enhance short wavelength anomalies while suppressing long wavelength components caused by deep-seated features and slow density variations, allowing more accurate lithological contact and edge detection. This is particularly useful in determining the existence and location of steeply dipping boundaries.

7. Euler Deconvolution

THOMPSON (1982) has described a technique based on Euler homogeneity equation to estimate depth from magnetic profiles. Euler deconvolution was later generalized by REID *et al*., (1990) for gridded data and yields the location and depth of the sources. This technique can be applied to gravity data as well (KEATING 1998). This method has proved to be very powerful in lineaments recognition and geological contacts and faults detection; it can be used to assist for fast interpretation of any potential field data terms

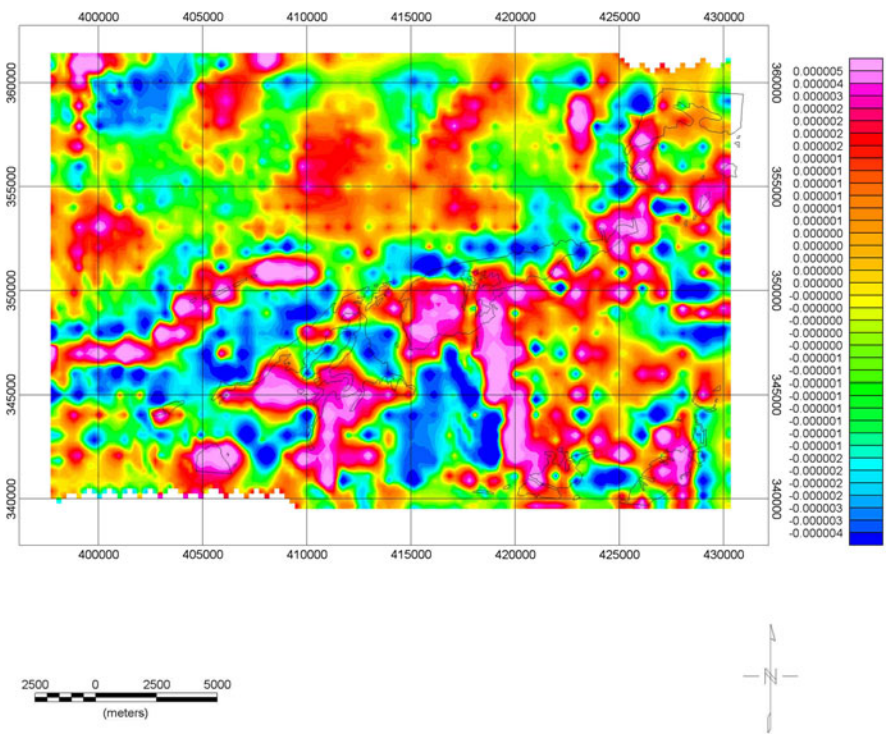

Figure 7
Second vertical derivative

for depth and geometry delineation of the structures. In the other hand, this method needs some refinement in order to keep the most useful solutions.

Euler deconvolution has been applied to both magnetic and gravity data over many years. It is based on Euler's homogeneity equation and can be expressed as follows:

$$(x - x_0)\frac{\partial T}{\partial x} + (y - y_0)\frac{\partial T}{\partial y} + (z - z_0)\frac{\partial T}{\partial z} = -N(T - B)$$

where (x_0, y_0, z_0) are the coordinates of the source; the total field T is measured at (x, y, z) and B is a local background; N indicates the structural index and relates to the rate of change of a potential field with distance.

Euler equation is solved within a moving window of the total field and its orthogonal derivatives. A least square solution gives (x_0, y_0, z_0) and uncertainties, for a given index N (Reid *et al.*, 1990). Solutions with a depth uncertainty (standard deviation) over a user defined threshold (tolerance) are rejected.

To obtain reliable results, the structural index, the window size and the tolerance have to be cautiously selected.

The structural index corresponding to the rate of change of the field depends on source geometry and can have a value from 0 to 3. The depth tolerance controls the accepted solutions, i.e. solutions are accepted with error estimate less than this tolerance. A smaller tolerance results in fewer but more reliable solutions. The window size determines the area in grid cells used to carry out Euler deconvolution. All points within the window are used to solve Euler's equation for source location. It should be large enough to incorporate the entire anomaly being interpreted and small enough to avoid significant effects from adjacent or multiple sources (Bournas *et al.*, 2003).

The deconvolution was applied to gravity field of the area of study. In this work, we have solved the equation with changing at each time a parameter and keeping the other parameters constant. The correct parameter is then selected by inspecting the maps deduced from each one and compared to the others, giving the tighter solutions clustering.

Before applying the Euler deconvolution to the area and in order to optimize the inversion, we have first determined the appropriate parameters. We started with the structural index SI. That is because the relation between the structural index and the subsurface geologic features forms the basis for the inversion process. This has been extensively discussed by Thomas *et al.*, (1992), and Reid *et al.*, (1990). For regional interpretation and taking into account the contact model, Reid *et al.*, (1990) have shown that the lower structural indices ranging from 0 to 1 are better depth estimators. The correct structural index is then chosen by inspecting maps deduced from each structural index, giving the tighter solutions clustering. In the present work, we have solved for the range of three indices (0, 0.5, and 1) and kept a constant window size ($W = 11$ grid cells) as well as threshold tolerance (TZ = 8). From the results presented in Fig. 8, for each structural index value, we deduct that structural indices 0.5 and 1 yield well non organized solutions (Fig. 8, A-2, A-3), especially in the southern part, while the highest structural index (SI = 1) yields overestimated depth solutions (Fig. 8, A-3). However, the best depth estimates and the tightest clustering of solutions are given with the structural index SI = 0 (Fig. 8, A-1).

The choice of the window size depends on the wavelength of the studied anomaly. Selecting a small window may result in poor definition of longer wavelength anomalies. On the other hand, choosing a large window leads to a risk of including the effects of multiple sources which may generate a cloud of poorly defined solutions that would mask the better ones. Solutions obtained with different window sizes ranging from 6×6 for the smallest (Fig. 8, C-1), to 16×16 for the largest are illustrated in Fig. 8, C-3. It is easy to notice that for the smallest window size only few solutions are represented and that the edges are poorly defined; whereas for larger window sizes a cloud of solutions is observed, causing bad source-bodies delineation and that some edges are weakly defined. However, the better solutions are obtained using a window size 11×11 (Fig. 8, C-2).

As Euler deconvolution yields a solution for each window size, it is necessary to reject solutions with higher uncertainties. This is controlled by fixing a threshold tolerance; whenever the depth error is greater than this value, the associated depth is automatically rejected. A Test using some tolerance

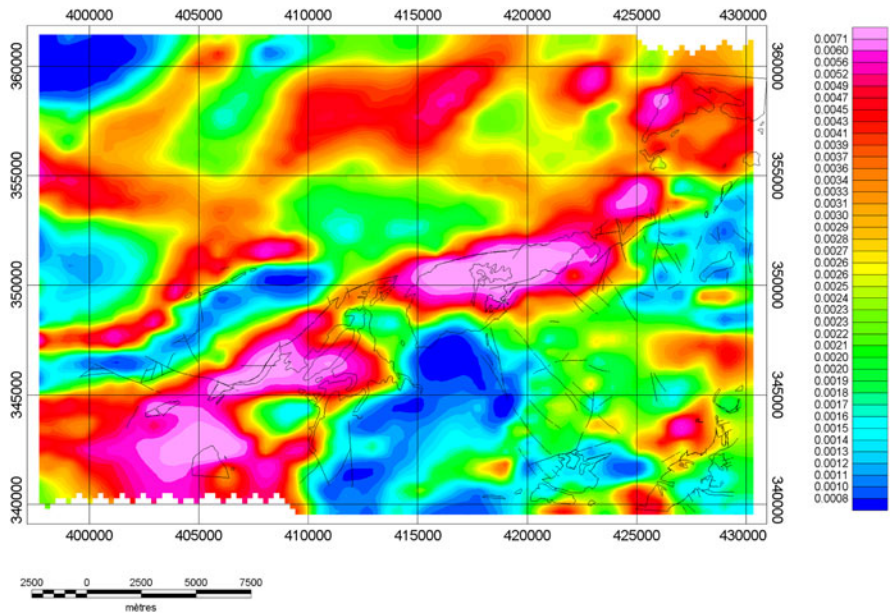

Figure 8
Horizontal gravity gradient

values is performed on our case. We have found that for tolerance as small as TZ equal 4, fewer reliable solutions are obtained (Fig. 8, B-1). However, increasing the tolerance yields to the production of more solutions, which mask the better ones. In our case, we find that the best solutions are inferred through the adoption of a tolerance value of 8 (Fig. 8, B-2).

Euler solutions presented in Fig. 8, C-2 were obtained for a structural index of zero; this value provides usually a reliable indication of large-scale faulting, a window size of 11×11 cells and a threshold tolerance of 8. The colored dots indicate the source edges, and each color is related to one of the estimated depths which are spread out in eight ranges (Fig. 8, C-2).

In the central eastern and southern regions, results correlate with the known geological contacts and faults. The positive anomaly, related to region one in Fig. 9, is bordered to the North by aligned solutions corresponding approximately to the Northern limit of the Triassic outcrop of J. Sidi Mahdi. The western limit corresponds to a NNW oriented aliened solutions which expresses a fault system in the same direction. The western part is limited by a NNE directed fault system that has not expression in the surface geology. To the southeastern part there is a NS fault system marked by the alignment of solutions that limits the Triassic outcrop of Fej Elhdoum to East. The southcentral part of the area, related to region 6, is contoured by a succession of solutions which indicate the contact between this negative anomaly and both bordering positive ones. These solutions are indication of faults system which orientation is well known in the geology of the Tunisia. In the southwestern part at J. Dardouria Triassic outcrop a NE deep fault is outlined.

To the North, near Kt. Berrebaane solutions mark out a NE directed fault which separate two domains of different density contrast.

Region 4 is delimited to North by a NE oriented fault system; to the east, it is bordered by NS fault which is not well expressed; its continuation to the south is not well defined trough this technique. However, the western limit is well marked by a NW oriented fault system. It was interpreted as a graben structure (Amiri 2008).

In the northern region the solutions indicate the presence of deep geological structures beneath Quaternary deposits. Therefore, tightest clustering solutions outline new faults affecting geological series under Quaternary deposits. Thus, El Mardja

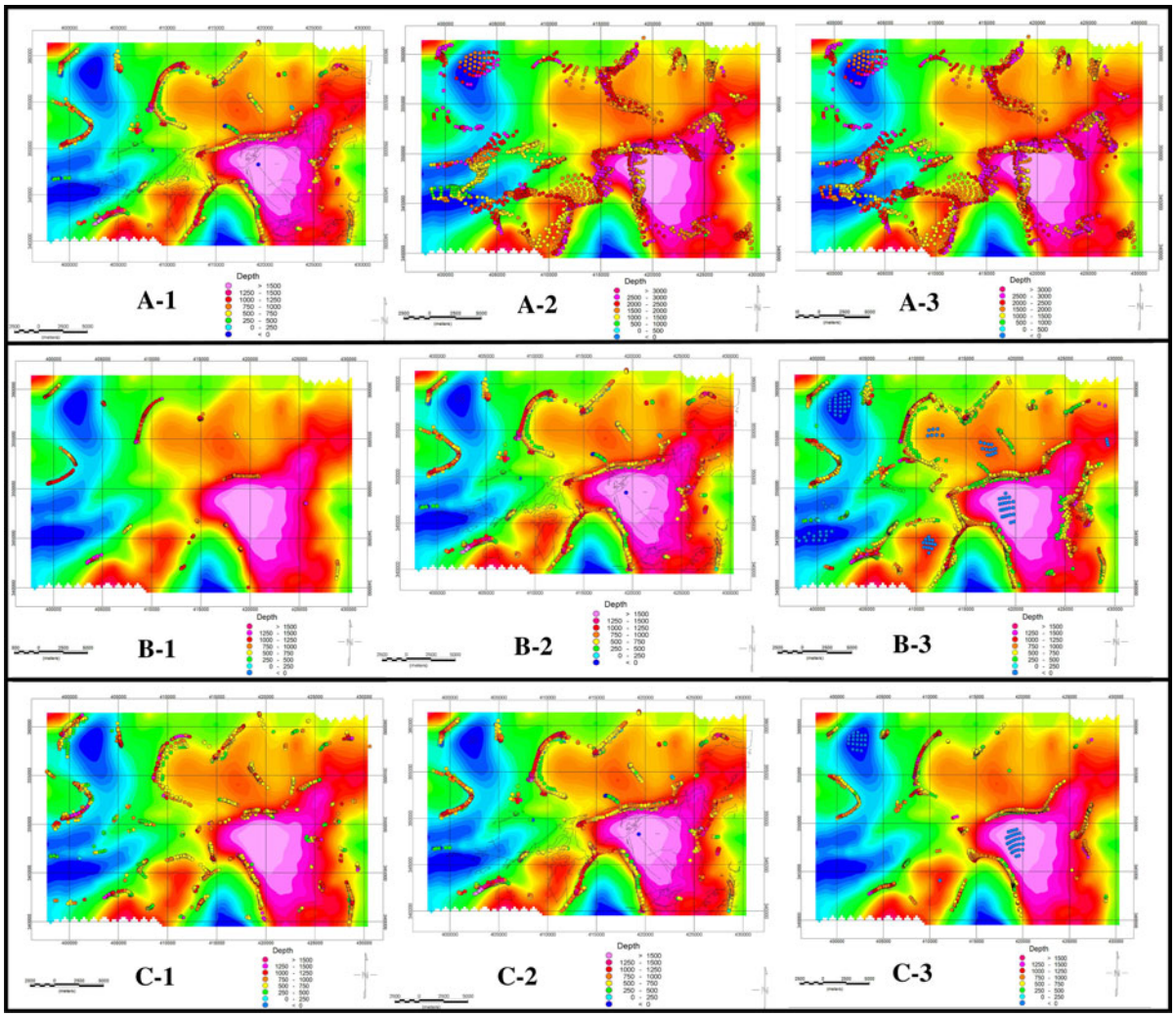

Figure 9

Results obtained with the Euler deconvolution superimposed on the Bouger gravity anomaly map. (*Black polygons* represent Triassic outcrops and *black lines* represent the known faults in the surface geology). **A-1** SI = 0, $T = 8$, $W = 11$; **A-2** SI = 0.5, $T = 8$, $W = 11$; **A3** SI = 1, $T = 8$, $W = 11$; **B1** SI = 0, $T = 4$, $W = 11$; **B2** SI = 0, $T = 8$, $W = 11$; **B3** SI = 0, $T = 12$, $W = 11$; **C1** SI = 0, $T = 8$, $W = 6$; **C2** SI = 0, $T = 8$, $W = 11$; **C3** SI = 0, $T = 8$, $W = 16$

anomaly is delineated by a series of faults behaving as an arched system.

8. *Bandpass Filtering*

Wavelength band-pass filtering is used in order to focus in some details within the area of study. Although the anomalies created by this technique cannot be attributed to either shallow and/or deep sources, they are useful in a qualitative sense in determining the origin and depth of the anomalies. Fig. 10 is a filtered gravity map where wavelengths in the range of 2,000–15,000 m were kept; all the others were rejected.

The important observation here is the existence of short and strong wavelength anomalies. El Mardja anomaly becomes a great circular one, separated from its adjacent anomalies. It would be the expression of hidden bodies with higher density. Lineaments outlined by Euler solutions coincide with the limits of this anomaly.

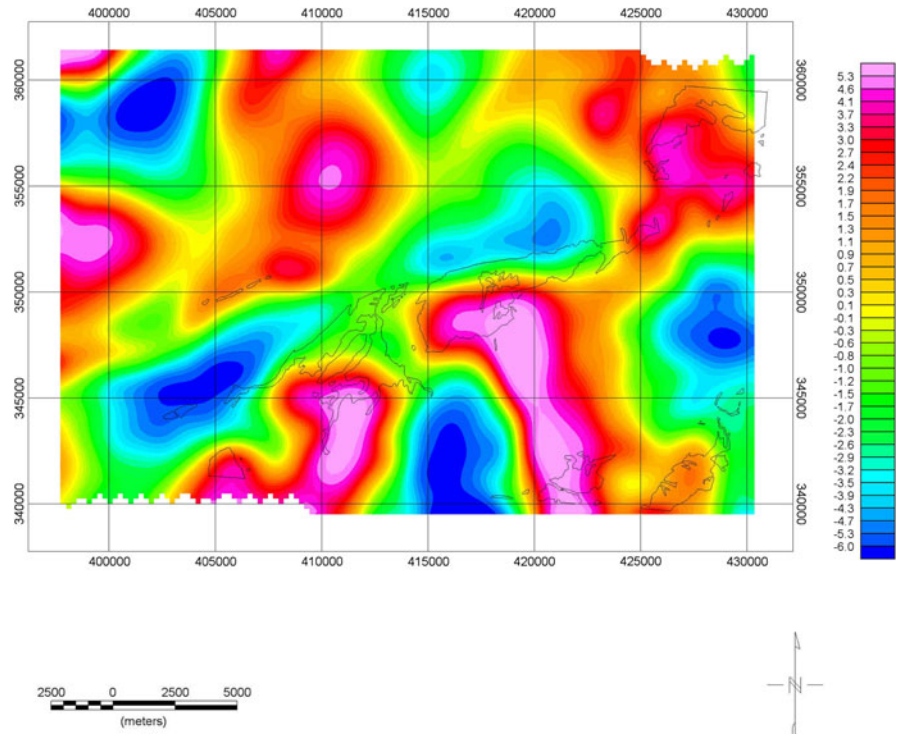

Figure 10
Band-pass filtered map where wavelengths between 2,000 and 15,000 km were passed

The area of study belongs to the "diapirc zone" of Northern Tunisia, which is characterized by numerous Triassic outcrops generally elongated with a NE bearing; they bear gypsum, clay, some metasomatized basalts (sills, dikes), sands as well as lime- and dolostones. Due to its heterogeneous mixture, Triassic material would be denser (Hamdi Nasr *et al*., 2007; Hamdi Nasr *et al*., 2009), leading to the observed positive gravity response (Hamdi Nasr *et al*., 2009; Benassi *et al*., 2006).

9. *Discussion and Results*

Gravity anomaly separation is defined as the separation of the gravity effects of deep geologic sources from the effects of shallow geologic sources. Residual field (Jacobsen, 1987) denotes the portion of the observed gravity field arising from shallow geologic sources. Regional field denotes the remaining portion of the observed gravity field caused by deep geologic sources.

The second vertical derivative allows the enhancement of the near surface density contrasts that expresses superficial geologic features. The susceptibility of the second derivative to noise and errors as well as topographic discontinuities is avoided with the aid of the horizontal gravity gradient (Butler, 1984); the extracted horizontal gravity gradients, which would be devoid of topographic influences, should better locate buried shallow masses than vertical gradient.

The amplitude and width of a second vertical derivative is higher and narrower than the first vertical gradient and thus, supposedly easier to interpret. So, lineaments are well expressed, e.g. J. Rharmanouba, J. Argoub Naoua. The vertical derivative technique allows the expression of all lineament trends; so, no filtering effect performed along a specific direction is performed as it is the case for HGG technique. In the mean time, HGG helps defining structural geology associated with a specific faulting/folding system of deformation: e.g. J. Zitoun-J. Sidi Mahdi, J. Rhdir el Kelba.

The EHD technique optimizes the signal to noise ratio and tends to raise signal amplitudes of short-wavelength compared to those of long-wavelength. Edges of density contrasts can be roughly seen as high positive amplitude values. The EHD reveals a variety of directions that correspond to the boundaries of structures; all the directions can be observed: NE, NW, EW and NS with dominance of the NE oriented alignment. This result is well confirmed by the HGG of which the EW and NE are the most enhanced directions, such as the NE directed lineament occurring over Triassic body of J. Zitoun-J. Sidi Mahdi, the NE lineament of J. Rharmanouba and the NE direction of Kt. Berrebaane. The horizontal gradient simply indicates the presence of a measure of the lateral change in density and requires no assumptions about the sources. Its magnitude is dependent on the density contrast across the domain boundary, the vertical extent of the contrast, the dip of the boundary and its depth of burial (Thomas *et al.*, 1992). The steepest horizontal gradient of a gravity anomaly will be located directly over the edge of the body if the edge is vertical and far removed from all other edges or sources (Thomas *et al.*, 1992).

Gravity anomaly separation using bandpass filtering is based on the tenet that a given geologic source's spectral power is attenuated more rapidly at high spatial frequencies than low spatial frequencies as the source depth increases (Pawlowski, 1994). Matched filtering (Syberg, 1972; Spector and Grant, (1970) is arguably the optimal way to do the bandpass separation for equivalent layers. Presumably, all responses of terrains (rock formations as well as lineaments, e.g. faults) shallower than 2,000 m as well as those deeper than 15,000 m are rejected.

The cumulative lineament map (Fig. 11) is obtained from merging lineaments that are evidenced by single Gravity component maps. The map expresses a synthetic overview of all available structures in the area. This map represents substantial knowledge improvement of the structures arrangement in the area.

It is sensitive to underline that the analyzed data set provides information on even subtle anomalies that would go undetected in the Bouguer anomaly map, where the effects of regional structures are predominant (Fedi *et al.*, 2005). The transformed gravity maps (residual component, derivative, and Euler deconvolution) enhance different trends with respect to others, depending on their spatial orientation and extension.

The geometrical structural features can be readily understood on the CLM. This is exemplified by the El Mardja anomaly with its perfect circular form (Figs. 3, 10), and the fact that is bordered by a "curved" fault system (Fig. 8). It represents the response of a Triassic dome well expressed by the positive density contrast of the Triassic material. Triassic material average density approximates 2.51 g/cm^3 (Onm, 2000; Arfaoui, 2004).

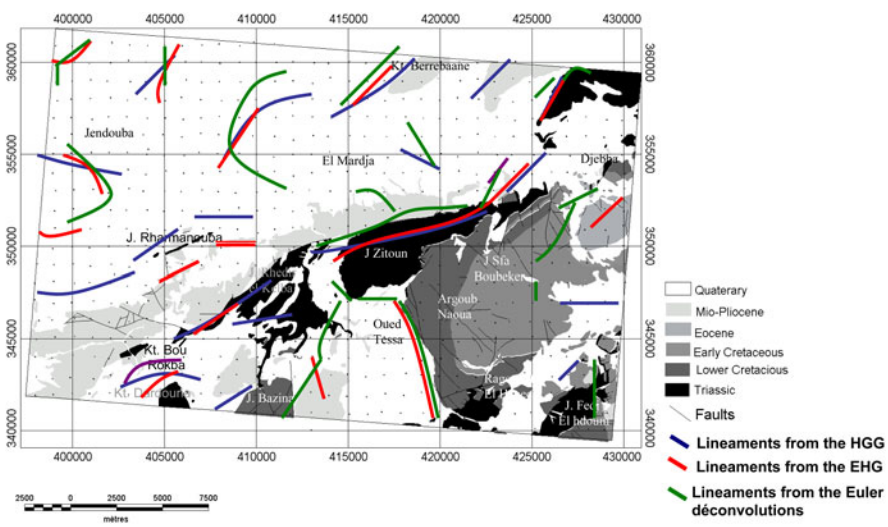

Figure 11
Cumulative lineaments map superimposed the geological map of the area

This bulk density value related to Triassic material is higher than the shallow bordering formations.

Gravity axes are located in zones of strong density contrast compared to that of the surrounding rock intervals. Gravity maps mark clear distinction of two quite domains separated by NE trending limit. This is recognizable by the topographic alignment of J. Sidi Mahi, J. Resfa, J. Zitonun, J. Rhedir EL Kalba, Kt. Bourokba. The most important variations are located in the half southern domain of the gravity maps.

To the North of the map and the south east of Kt Berrebane there is a NE oriented lineament. It can be a Fault characterized by a marked gravity boundary. It is revealed by the Euler deconvolution method. Its estimated depth would be between 500 and 750 m for the central part, both borders would be deeper.

The western part of the lower Cretaceous of Argoub Naoua, which corresponds to the eastern part of Ouet Tessa, is marked by a NS to NNW oriented fault system which is 500–1,000 m deep. This fault separates the lower Cretaceous from the Quaternary deposits. It may be a limit of a depressed recent structure covered by quaternary deposits. This fault may be the northeastern border of a graben structure. The western limit of Oued Tessa is marked by a NE to NNE fault system deeper than the eastern one 1,000–1,250 m. This fault limits the Triassic of J. Rhedir el Kelba and the Lower Cretaceous of J. Basina.

Gravity gradient maps show that the Triassic outcrops of J. Rharmanouba correspond to gravity lineaments oriented NNE. It continues to the West and the direction becomes EW.

All these directions, recognizable in Northern Tunisia (Crampon, 1973; Rouvier, 1977; Perthuisot, 1978; Chihi, 1995; Ben Ayed, 1986), are evidenced by our gravity analysis in Jendouba area.

As a matter of fact, the CLM provides more information than surface geological map, so that structures arrangement would be better approached in the 3-D volume.

Acknowledgments

We are indebted to Doctor Abdelbaki Mansouri and to Professor Pierre Keating for constructive criticism of the original version of this manuscript. We wish to thank Professor Steven D. Sheriff and an anonymous reviewer, as well as Professor Eugenio Carminati for constructive reviews and comments which helped to improve the paper substantially.

References

Amiri,, A. (2008), Apport de la gravimétrie dans la caractérisation des structures géologiques de la moyenne vallée de la Medjerda. Modélisation des séries mioplio- quaternaires des la moyenne vallée de la Medjerda. Mémoire de mastère, Univ. Tunis II, Faculté des sciences de Tunis. 85 pp

Arfaoui, M. (2004), Expression gravimétrique et interprétation structurale multi- scalaire dans la région du Kef- Ouargha. Mémoire de mastère. Faculté des sciences de Tunis, 125 pp

Ben Ayed, N. (1986), Evolution tectonique de l'avant-pays de la chaine alpine de Tunisie du début du Mésozoique 'a l'Actuel. PhD thesis, Université de Paris Sud, Centre d'Orsay

Ben Haj Ali, M. (1979), Etude géologique du Jebel Goraa (Région de Teboursouk, Atlas tunisien). Thèse de 3ème cycle, Université de Paris VI

Ben Haj Ali, et al. (1997), Carte géologique au 1/50,000 de la région de Jandouba. Direction des Mines et de la géologie, Ministère de l'Industrie des mines et l'Energie, Tunisie

Benassi R., Jallouli, C., Hammami, M., and Turki, M. M. (2006), The structure of Jebel El Mourra, Tunisia: a diapiric structure causing a positive gravity anomaly. Terra Nova *18*, 432–439

Blakely, R. J., *Potentiel theory in gravity and magnetic applications*. (Cambridge University Press 1996) 441 pp

Blakely, R., Simpson, R. (1986), *Approximating edges of sources bodies from magnetic or gravity anomalies*. Geophysics *51*, 1494–1498

Bournas, N., Galdeano, A., Mohamed M., Baker, H. (2003), *Interpretation of the aeromagnetic map of Eastern Hoggar (Algeria) using the Euler deconvolution, analytic signal and local wavenumber methods*, J Afr Earth Sci *37*, 191–205

Buness, H., Giese, P., Bobier, C., et al. (1992), *The EGT'85 seismic experiment in Tunisia: a reconnaissance of deep structures*, Tectonophysics *207*, 245–267

Butler, D. K. (1984), *Gravity gradient determination concepts*, Geophysics *49*, 828–832

Castany, G. (1952), Paléogéographie, tectonique et orogenèse de la Tunisie. Monographies régionales. 2ème série: Tunisie-N°1

Chihi, L. (1995), Les fossés néogènes à quaternaires de la Tunisie de la mer pélagienne: leur signification dans le cadre géodynamique de la méditerranée centrale. Thèse de Doctorat d'Etat, Université de Tunis II, 324 pp

Cohen, C. R., Schamel, S., Boyd-Kaygi, P. (1980), *Neocene deformation in Northern Tunisia: origin of the eastern Atlas by microplate-continental collision*. Geol Soc Am Bull *91* 205–237

Cooper, G. R. J., and Cowan, D. R. (2006), *Enhancing potential field data using filters based on the local phase*, Comput Geosci *32*, 1585–1591

Crampon, N. (1973), Disposition et modalités de mise en place du complexe salifère M. Solignac. Annales des Mines et de la Géologie, Tunis *26*, 269–272

Fairhead, J. D., and Williams, S. E. (2006), *Evaluating normalized magnetic derivatives for structural mapping*. SEG Expanded Abstracts 25, 845 pp

FEDI, M., and FLORIO, G. (2001), *Detection of potential fields source boundaries by enhanced horizontal derivative method*. Geophys Prospect *49*, 40–58

FEDI, M., FLORIO, G., and CELLA, F. (2007). Toward a full multiscale approach to interpret potential fields, EGM 2007. International workshop innovation in EM, Grav and Mag Methods: a new perspective for exploration Capri, Italy

FEDI, M., FERRANTI, L., FLORIO, G., GIORI, I., ITALIANO, F. (2005), *Understanding the structural setting in the Southern Apennines (Italy): insight from Gravity Gradient Tensor*. Tectonophys *397*, 21–36

GUPTA, V. K., and RAMANI, N., (1980). *Some aspects of regional-residual separation of gravity anomalies in a Precambrian terrain*. Geophysics *45*, 1412–1426

HAMDI NASR, I., BEN SALEM, A., INOUBLI, M. H. (2007), Gravity analysis of Jbel Cheid (Northern Tunisian Atlas). International workshop innovation in EM, Grav and Mag methods: a new perspective for exploration Capri, Italy

HAMDI NASR, I., BEN SALEM, A., INOUBLI, M. H., DHIFI, J. ALOUANI, R., CHAQUI, A. PETHUISOT, V. (2008), Apports de la gravimétrie dans la caractérisation des structures éffondrées dans la région de Nebeur (Nord Ouest de la Tunisie). Swiss J Geosci 101, 17–27

HAMDI NASR, I., INOUBLI, M. H., BEN, SALEM, A., TLIG, S., and MANSOURI A. (2009), *Gravity contributions to the understanding of salt tectonics from the Jebel Cheid area* (*dome zone, Northern Tunisia*) Geophys Prospect *57*, 719–728

HAMMER, S., (1939), Terrain corrections for gravimeter stations. Geophysics *4*, pp. 184–194

INOUBLI, M. H. and MANSOURI, A. (2006), Apport de la Gravimétrie dans la caractérisation des Modèles de Mise en Place des Structures triasiques à Caractère Extrusif. African Geology colloquium: CAG 21, Maputo–Mozambique

JACOBSEN, B. O. (1987) *A case for upward continuation as a standard separation filter for potential-field maps*. Geophysics *52*, 1138–1148

JALLOULI, C., et al. (2002), *Gravity constraints on the structure of the northern margin of Tunisia: implications on the nature of the northern African Plate boundary*, Geophys J Int *151*, 117–131

JALLOULI, C., CHIKHAOUI, M., BRAHEM, A., TURKI, M. M., MICKUS, K., and BENASSI, R. (2005), Evidence for Triassic salt domes in the Tunisian Atlas from gravity and geological data. Tectonophysics *396*, 209–225

KEATING, P. B. (1998), *Weighted Euler deconvolution of gravity data*. Geophysics *63*, 1595–1603

ONM (2000), Campagne gravimétrique CG3: Coupures 1/50000 de Nebeur, Jendouba, Saline et Teboursouk

PAWLOWSKI, R. S. (1994), *Green's equivalent-layer concept in gravity band-pass filter design*. Geophysics *59*, 1, 69–76

PERTHUISOT, V., (1978), Dynamique et pétrogène se des extrusions triasiques en Tunisie septentrionale. Thèse de doctorat d'état, Ecole Normale Supérieure, Paris.12 (312 pp)

PHILLIPS, JD., HANSEN, R. O., and BLAKELY, R. J. (2007), The use of curvature in potential-field interpretation. Explor Geophys *38*, 111–119

REID, A. B., ALLSOP, J. M., GRANSER, H., MILLETT, A. J., SOMERTON, I. W. (1990), *Magnetic interpretation in three dimensions using Euler deconvolution*. Geophysics *55*, 80–91

ROBINSON, D et al. (2007), Spectral analysis of gravity data in Tunisia. Geological Society of America, 41st Annual Meeting (11–13 April 2007)

ROUVIER, H. (1977), Géologie de l'extrême Nord tunisien: tectonique et paléogéographie superposées à l'extrême orientale de la chaine nord maghrébine. PhD thesis, Université de Paris VI

SPECTOR, A. and GRANT F. (1970), *Statistical models for interpreting aeromagnetic data*. Geophysics *35*, 293–302

SYBERG, F. J. R. (1972), A Fourier method for the regional-residual problem of potential fields. Geophys Prospect *20*, 47–75

THOMAS, M. D., GRIEVE, R. A. F., SHARPTON, V. L., Structural fabric of the North American continent, as defined by gravity trends. In: *Basement tectonics* (ed. Mason R) (Kluwer Academic Press 1992)

THOMPSON, D.T., (1982), EULDPH - a new technique for making computer-assisted depth estimates from magnetic data: Geophysics *47*, 31–37

TLIG, S., ERRAOUI, L., BEN AISSA, L., ALOUANI, R., TAGORTI, M.A., (1991), Tectogenèses alpine et atlasique: deux événements distincts de l'histoire géologique de la Tunisie. Corrélation avec des événements clés de la Méditerranée. C. R. Acad Sci., Paris Série II *312*, 295–301

VERDUZCO, B., et al. (2004), *New insights into magnetic derivatives for structural mapping*. The Leading Edge *23*, 116–119

(Received July 2, 2009, revised July 8, 2010, accepted July 15, 2010, Published online August 31, 2010)